Science of the Total Environment 794 (2021) 148573

Contents lists available at ScienceDirect

Science of the Total Environment

journal homepage: www.elsevier.com/locate/scitotenv

Acoustic scattering by gas-bearing cyanobacterium *Microcystis*: Modeling and in situ biomass assessment

Dezhang Chu [a,*], Ilia Ostrovsky [b,*], Hikaru Homma [b]

[a] Fishery Resource Analysis and Monitoring Division, Northwest Fisheries Science Center, National Marine Fisheries Service, National Oceanic and Atmospheric Administration, 2725 Montlake Boulevard East, Seattle, WA 98112, USA
[b] Israel Oceanographic and Limnological Research, Yigal Allon Kinneret Limnological Laboratory, P.O. Box 447, Migdal 1495000, Israel

HIGHLIGHTS

- Vertical distribution of cyanobacteria *Microcystis* is detectable with echosounder.
- Acoustic scattering and regression models allow quantifying *Microcystis* biomass.
- Acoustics is a powerful tool for rapid monitoring of gas-bearing cyanobacteria.

GRAPHICAL ABSTRACT

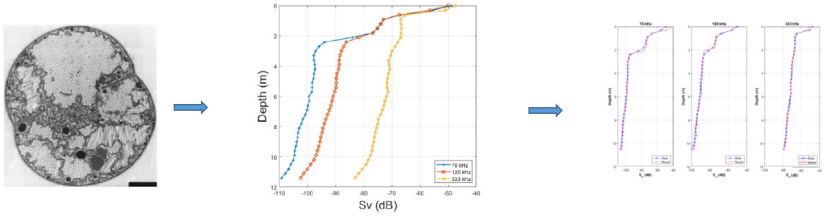

A single cell of cyanobacterium *Microcystis*

Profiles of acoustic backscatter of *Microcystis* at 70, 120, 333 kHz

Comparison of acoustic data and scattering model predictions at 70, 120, 333 kHz

ARTICLE INFO

Article history:
Received 2 April 2021
Received in revised form 15 June 2021
Accepted 16 June 2021
Available online 22 June 2021

Editor: Jay Gan

Keywords:
Cyanobacterium *Microcystis*
Echosounder
Acoustic backscattering
Partially coherent scattering
Biovolume concentration

ABSTRACT

Cyanobacterial harmful algal blooms (HABs) are increasing in a growing number of aquatic ecosystems around the world due to eutrophication and climatic change over the past few decades. Quantitative monitoring of HABs remains a challenge because their distributions are spatially heterogeneous and temporally variable. Most of the standard biological sampling methods are labor intensive and time consuming. In this paper, we present an efficient acoustic method to assess the biomass (biovolume) concentration of the cyanobacterium *Microcystis* in aquatic ecosystems. Acoustic backscattering vertical profiles from a gas-bearing *Microcystis* population were measured with echosounders at three frequencies (70, 120, and 333 kHz) in Lake Kinneret (case study). Concurrently, the volume concentration of *Microcystis* colonies and cyanobacteria-related Chlorophyll *a* were evaluated. We developed a partially coherent acoustic scattering model to quantify the cyanobacterium biomass based on depth-dependent acoustic backscattering signals. We also evaluated empirical regression models to obtain the *Microcystis* biomass from acoustically measured volume backscattering strength, S_v. It is demonstrated that both methods can convert the S_v to *Microcystis* biovolume concentrations reasonably well. Pro and cons of these methods are discussed. The results suggest that the presented methods may have a potential to be used for broader applications to monitor and quantify the gas-containing plankton in large aquatic ecosystems.

1. Introduction

Cyanobacterial harmful algal blooms (HABs) are increasing in a growing number of aquatic ecosystems all around the world due, in part, to eutrophication and climatic change (Markensten et al., 2010;

* Corresponding authors.
E-mail addresses: Dezhang.chu@noaa.gov (D. Chu), ostrovsky@ocean.org.il (I. Ostrovsky).

https://doi.org/10.1016/j.scitotenv.2021.148573

Paerl and Paul, 2012). HABs disrupt the functioning of lake ecosystems and potential water use because many cyanobacterial species can produce toxic metabolites which can be harmful to humans and animals (Codd et al., 2005). Toxic *Microcystis*, one of the most common and ubiquitous cyanobacterial genera, frequently blooms in lakes and reservoirs (Reynolds et al., 1987; Huisman and Hulot, 2005). Many countries have developed studies and implemented monitoring programs aimed at detection of early stages of bloom development and understanding the factors affecting cyanobacteria blooms. Highly heterogenic spatial distribution of the buoyant cyanobacteria in water bodies is the major challenge for reliable monitoring of these organisms. Floating cells and colonies may form patches and accumulate at certain peripheral locations resulting from water motion (Pobel et al., 2011; Clark et al., 2017).

While development of efficient and effective methods for investigating cyanobacterial blooms has become an important issue over the last few decades, there are still no satisfactory quantitative methods for fast and accurate 3-dimensional monitoring of the spatiotemporal distribution of the cyanobacterial bloom. Most available biological sampling methods are labor intensive and time consuming. Developing an efficient and accurate method for properly monitoring cyanobacterial biomass in a rapidly varying and spatially heterogeneous environment is challenging. Satellite or drone-based remote sensing is an efficient and non-invasive technology of estimating cyanobacterial biomass, which can provide a good spatial coverage and allow studying the phytoplankton patchiness based on images of water surface optical properties (Kim et al., 2018; Mishra et al., 2019). However, these methods cannot accurately evaluate the areal integrated biomass (per square meter) due to large heterogeneity in vertical distributions of buoyant cyanobacteria caused by spatially variable vertical turbulent mixing. For instance, in more quiet areas the buoyant cyanobacteria are predominantly concentrated near the water surface, while in other locations they can be dispersed vertically by wind-driven turbulence and, thus, may have low near-surface biomass despite of large vertically integrated biomass. Therefore, new methodologies are ultimately needed for research and monitoring.

Acoustics, one type of remote-sensing technology, facilitates rapid, quasi-synoptic surveys of large volumes of water. Scientific echosounders provide high-resolution data on organism abundance in both space and time, and have been widely used to quantify fish, zooplankton (Huber et al., 2011; Simmonds and MacLennan, 2005; Stanton et al., 1994, 1998), and gas bubbles (Ostrovsky, 2003; Ostrovsky et al., 2008). Small gas-bearing fish larvae and zooplankton are strong sound scatterers, thus can be detected with echosounders and Acoustic Doppler Current Profilers (Lorke et al., 2004; Potiris et al., 2018). Recent studies have shown that spatial and temporal variability of gas-containing cyanobacteria can also be studied with acoustic devices at ultrasonic frequencies (Ostrovsky et al., 2017, 2018; Godlewska et al., 2018; Hofmann and Peeters, 2013). Strong correlations between volume backscattering coefficient and biomass of gas-bearing *Microcystis* have been revealed in tank experiments and in a shallow lake (Ostrovsky et al., 2020). Still, preliminary data collected with a 120 kHz echosounder on Lake Kinneret (Israel) displayed the presence of a sharp boundary between the highly echo-reflecting upper layer and deeper strata (Ostrovsky et al., 2017) that implied a mismatch between the smoothly distributed cyanobacterium biomass and backscattering signal. It was noted that such a boundary was positioned in proximity to the diurnal thermocline, which allowed the large buoyant colonies to concentrate in the upper stratum, usually within a couple of meters from the surface (Ostrovsky et al., 2020).

Like some other cyanobacteria, *Microcystis* contains gas vesicles (GV) which help regulate cell or colony buoyancy and manage their position in the water column. Formation of GV might be regulated by light levels, but other environmental factors, such as temperature, salinity, pH, and anoxic conditions, may also affect GV formation (e.g. Pfeifer, 2012). GV are aggregated in gas vacuoles of irregular shape within the cell (Walsby, 1994), while *Microcystis* cells form colonies of different sizes and often complex shapes. The presence of gas-containing structures drastically increases the backscattering intensities of planktonic organisms (Lavery et al., 2010; Martin et al., 1996; Stanton et al., 1994).

Studies of the acoustic properties of gas-bearing cyanobacteria are very limited. Recent investigations of frequency-dependent backscattering of rod-shaped gas vesicles from the cyanobacterium *Anabaena flos-aquae* revealed two resonance peaks (120 and 85 MHz), which demonstrated that their acoustic behavior was different from that of microbubbles (Yang et al., 2017). Acoustic properties of *Microcystis* colonies are difficult to deduce from properties of their components. When scatterers are closely packed together, their scattered fields strongly interact at particle separations much less than a wavelength, e.g. for a 120 kHz echosounder at distances $<<1.25$ cm. For randomly packed units, a cluster behaves as a pressure release surface, and sound reflection takes place at this interface (Clay and Medwin, 1977). Thus, the scattering cross sections of a small GV-containing cell, cell-containing colony, and closely spaced population of colonies are not equal to the arithmetic sums of the cross sections of their respective components. While many efforts have been made to study the physical characteristics of *Microcystis* colonies, their backscattering acoustic properties are still unknown. The objectives of this work are to model the acoustic properties of *Microcystis* colonies at three ultrasonic frequencies, compare the model results with in situ measurements, and to study the relationship between the acoustic backscattering signal and cyanobacterium biomass proxies, such as biovolume concentration (VC) and *Microcystis* associated chlorophyll *a* (Chl a_{Micro}) concentration in deep Lake Kinneret (Israel).

2. Materials and methods

2.1. Morphology of cyanobacteria Microcystis

Microcystis sp. forms colonies of various sizes, each consisting of a few to thousands of spherical cells. These cells contain closely packed or stacked cylindrical gas vesicles with conical end caps, or spindles, as shown in Fig. SM1-1a (Walsby, 1994; Park and Kim, 2017) in Supplementary Material (hereafter SM). In freshwater cyanobacteria, the length of these vesicles, L_c, varies from 100 nm to more than 800 nm and the diameter (width) of these cylinders (spindles), $2a_c$, (where a_c is the cylindrical radius) varies from 62 nm to 84 nm (Fig. SM1-1b). One of the interesting aspects of these vesicles is that within each species the width of these spindles is quite uniform with a standard deviation of only about $\pm 4\%$ (Walsby, 1994).

2.2. Acoustic modeling of backscattering by cyanobacteria Microcystis

In this study, we model the backscattering characteristics of cyanobacteria *Microcystis* using the method that is elaborated for fisheries acoustics at common frequencies from 10's to 100's kHz. For commercial fisheries echosounders, the scattering of a single *Microcystis* vesicle (diameter $\ll 1$ μm) is well within the Rayleigh scattering region, much lower than the vesicle (bubble) resonance frequency (Yang et al., 2017). More specifically, $\sigma_{bs} \propto f^4 V_{ves}^2$, where σ_{bs} is the differential backscattering cross section of a single gas vesicle, f is the acoustic frequency, and V_{ves} is the volume of a single vesicle. In other words, the backscattering is insensitive to the shape but sensitive to the volume of vesicles. As a result, without loss of generality, we can approximate the spindle-shaped vesicle to an equivalent spherical shell of equal volume (Cherin et al., 2016) as shown in Fig. SM1-1b (Walsby, 1994; Park and Kim, 2017).

The typical length and width of these vesicles are about 500 nm and 64 nm, and the thickness of the shell is about 1.8 *nm* (Walsby, 1994), i.e. the mean equivalent spherical radius is about 70 nm. Since these vesicles are densely packed (cohered) in each cyanobacteria cell, the scattering by a single cell is a coherent summation of all the vesicles within the cell in the sense that the phase differences between their individually scattered waves are very small compared to the acoustic wavelength. Similarly, since *Microcystis* cells are aggregated in colonies

of various sizes and different (random) separation distances, at any frequency the acoustic scattering by colonies with lower densities is less coherent than that with higher densities (Ishimaru, 1978). Consequently, the overall scattering by cyanobacteria cells and colonies is expected to be neither completely coherent nor completely incoherent. In addition, the multiple scattering is also inevitably involved. Scattering models describing multiple scattering are available in literature (Ishimaru, 1978; Hahn, 2007; Kouzoubov, 2018). However, due to an extremely large number of vesicles involved in the current scattering problem (>10^{11}), it becomes extremely difficult to accurately evaluate the multiple backscattering by these aggregated air-bearing cyanobacteria *Microcystis* (e.g. solving the exact integral equation). Here, we propose a simpler heuristic/empirical approach to characterize their acoustic scattering based on the following assumptions:

a. A general form of the backscattering by n targets of the same size is expressed as:

$$\sigma_{bs} = n^p |f_{bs}|^2$$

where σ_{bs} is the differential backscattering cross section, f_{bs} is the scattering amplitude of each single gas vesicle, and n is the number of targets. The power term p varies from 1 for complete incoherent scattering to 2 for complete coherent scattering (Gordon, 1958; Morse and Ingard, 1986; Akkermans et al., 1986);

b. Within an individual *Microcystis* cell, the total scattering is a coherent summation of the scattering by all gas vesicles;
c. The packing factor in *Microcystis* cells is a constant, i.e. vesicles do not collapse at the deepest depth the measurements were made (~12 m);
d. Scattering contributions by gas-bearing *Microcystis* cells within a colony and among colonies are partially coherent and the degree of the coherence depends on the volume concentration of the *Microcystis* cells;
e. Multiple scattering among gas vesicles (scattering by a single target more than once, Ishimaru, 1978; Colton and Kress, 2019), cells, and colonies is accounted for by using empirically fitted power, p, described above.

Based on assumption b, the differential backscattering cross section (σ_{bs}) of a single cell can be expressed as

$$\sigma_{bs}(f, \bar{a}_{cell}) = |n_{ves} f_{bs}(f, a_s)|^2, \quad (1)$$

where $f_{bs}(f,a_s)$ is the scattering amplitude of a single elastic spherical shell that can be modelled exactly (Goodman and Stern, 1962; Kargl and Marston, 1989), n_{ves} is the number of gas vesicles in a single *Microcystis* cell with an equivalent spherical radius, a_s (Fig. SM1-1b), and $\bar{a}_{cell}$ is the mean radius of *Microcystis* cells. A power of two states that the scattering by n_{ves} vesicles is purely coherent. The average σ_{bs} over the measured size distribution of *Microcystis* cells is

$$\langle \sigma_{bs}(f, \bar{a}_{cell}) \rangle_{a\,cell} = \sum_{n_b=1}^{N} \sigma_{bs}(f, a_{cell}) P_d(a_{cell}(n_b)) \quad (2)$$

where $a_{cell} = n_b \Delta a$, $P_d(a_{cell})$ is the probability of cell radius between $\left[a_{cell} - \frac{\Delta a}{2}, a_{cell} + \frac{\Delta a}{2}\right]$, with Δa is the size bin of cell radius, and N is the total number of bins in cell radius distribution. The predicted mean target strength (TS) is defined as $\langle \sigma_{bs} \rangle$ given by Eq. (2) expressed in the logarithmic domain (Simmonds and MacLennan, 2005):

$$\langle TS(f, \bar{a}_{cell}) \rangle_{a\,cell} = 10 \log_{10} \langle \sigma_{bs}(f, \bar{a}_{cell}) \rangle_{a\,cell} \quad (3)$$

The volume backscattering coefficient, an averaged quantity of σ_{bs} per unit volume (Simmonds and MacLennan, 2005), can be expressed by the following equation but with a power term $p(f,z)$ that is, in general, different from unity:

$$\langle s_V(f,z) \rangle_{a_{cell}} = n_{cyan}^{p(f,z)}(z) \langle \sigma_{bs}(f, \bar{a}_{cell}) \rangle_{a_{cell}} \quad (4)$$

where s_V is the volume backscattering coefficient at depth z (positive downward), $n_{cyan}(z) = n_{cell}(z) n_{col}(z)$ is the total number of cells per unit volume; n_{cell} and n_{col} are the mean number of cells in each colony and the number of colonies per unit volume, respectively. $p(f,z)$ is the power of n_{cyan}, which is a function of acoustic frequency and depth described by

$$p(f,z) = \begin{cases} p_0 & z > z_{ref} \\ p_0 + \alpha_0 \left(\frac{f_{ref}}{f}\right) \left(\frac{n_{cyan}(z)}{n_{cyan}(z_{ref})}\right)^{\frac{1}{3}} & z \le z_{ref} \end{cases}, \quad (5)$$

where p_0 and α_0 are empirically determined scaling coefficients by fitting to the acoustic data, and z_{ref} is the reference depth that can also be determined empirically by fitting the acoustic data. When $z < z_{ref}$, much stronger coherent and multiple scatterings start to affect the backscattering signal. When $z > z_{ref}$, the power term $p(f,z)$ in Eq. (4) is a constant (p_0), which is independent of frequency and a little larger than unity, representing a constant (partial) coherent contribution by cells in the colonies. However, when $z < z_{ref}$, $p(f,z) > p_0$, additional coherent contribution term depicts the impact of the adjacent colonies that are closely spaced. f_{ref} is the reference frequency, which in this study was chosen to be 120 kHz. The power $p(f,z)$ can vary between 1 (totally incoherent) and 2 (totally coherent). The term of $n_{cyan}^{1/3}(z)$ represents the number of cells per unit length (1 m), such that $n_{cyan}^{-1/3}(z)$ is then proportional to the average distance between the adjacent cell centers. Since acoustic wavelength, λ, is proportional to the inverse of frequency ($\lambda \propto f^{-1}$), the term of $f^{-1} n_{cyan}^{1/3}(z)$ reflects the number of *Microcystis* cells per wavelength.

The mean volume backscattering strength, S_v, is defined as (Simmonds and MacLennan, 2005):

$$S_v(f,z) = 10 \log_{10} \langle s_V(f,z) \rangle_{a\,cell} \quad (6)$$

The mean difference between the measured and modelled S_v, $\langle \Delta S_v \rangle$, where $\Delta S_v = S_v^{model} - S_v^{data}$, and the root-mean-square error of ΔS_v, ϵ_{rms}, over all depths provide a means to access the goodness of fit:

$$\langle \Delta S_v \rangle = \frac{1}{N_z} \sum_{i=1}^{N_z} \Delta S_v(z_j) = \frac{1}{N_z} \sum_{i=1}^{N_z} \left[S_v^{model}(z_j) - S_v^{data}(z_j) \right]$$
$$\epsilon_{rms} = \sqrt{\frac{1}{N_z} \sum_{i=1}^{N_z} |\Delta S_v(z_j)|^2} = \sqrt{\frac{1}{N_z} \sum_{i=1}^{N_z} \left[S_v^{model}(z_j) - S_v^{data}(z_j) \right]^2}, \quad (7)$$

where z_j corresponds to the j^{th} depth bin, and N_z is the total number of depth bins.

2.3. Estimation of biovolume concentration and biomass

The compact biovolume concentration, $V_{bio\_compact}$ that is made up of these compact *Microcystis* cells (packing factor of 100%), is the product of the mean volume of *Microcystis* cells and the number of cells in a unit of water volume. By applying Eqs. (4)–(6), $V_{bio\_compact}$ is then

$$\begin{aligned} V_{bio\_compact} &= \langle v_{cell} \rangle n_{cyan} \\ &= \langle v_{cell} \rangle \left(\frac{\langle s_V(f,z) \rangle_{a\,cell}}{\langle \sigma_{bs}(f, \bar{a}_{cell}) \rangle_{a_{cell}}} \right)^{1/p(z,f)} \\ &= \langle v_{cell} \rangle \left(\frac{10^{S_v(f,z)/10}}{\langle \sigma_{bs}(f, \bar{a}_{cell}) \rangle_{a_{cell}}} \right)^{1/p(z,f)} \end{aligned}, \quad (8)$$

Eq. (8) relates the ($V_{bio\_compact}$) and acoustic quantity S_v explicitly. The average volume of an individual *Microcystis* cell can be approximated by the volume of a sphere:

$$\langle v_{cell} \rangle = \frac{4\pi}{3} \bar{a}_{cell}^3, \tag{9}$$

with an average measured cell radius, $\bar{a}_{cell} = 1.4$ μm.

In reality, *Microcystis* volume concentration (VC) in this study was measured with the LISST-100× (Laser In-Situ Scattering and Transmissometry, Sequoia Scientific, Inc.), an instrument that can measure the sum of volume concentrations of *Microcystis* colonies, i.e. cell aggregates (see below). Since the colonies are loosely packed by cells (i.e. there are large distances between cells in the colonies), the sum of cell volumes can be notably lesser than the measured biovolume of colonies. A packing factor (ϕ_p) is used in the calculation of cell-based biovolume, which takes into account the loosely packed cells, with $\phi_p \propto \left(\frac{\langle d_{cell} \rangle}{\langle dist_{cell} \rangle}\right)^3$, where $\langle d_{cell} \rangle = 2\langle a_{cell} \rangle$ is the mean cell diameter, and $\langle dist_{cell} \rangle$ is the mean distance between the cell centers in a colony. Packing factor was evaluated as the average of several measurements in colonies of different sizes. In our model we used this measure as spatially invariable to simplify the scattering model. As a result, the measured VC and $V_{bio\_compact}$ estimated from Eq. (8) can be associated as

$$\mathrm{VC} = V_{bio\_compact}/\phi_p \tag{10}$$

The areal volume concentration (AVC) is defined as the vertical integration of the VC over the entire water column and has a unit of mL m^{-2}.

2.4. Field data collection

This study was carried out in the middle of the *Microcysits flos-aquae* bloom season. The measurements were conducted on *Microcystis* patches from 15:35 to 15:46 at Israel Summer Time (UTC + 03:00) on 3 Apr and from 15:25 to 15:52 on 4 Apr 2019 at the northwestern part of Lake Kinneret. More detailed information of the study area and some of the limnological characteristics are described in SM2.

2.4.1. Acoustic data

Acoustic data were collected with Simrad EK80 echosounders that consisted of the Wideband Transceiver Tube and three transducers. The echosounder was equipped with two echosounder boards; each of them contains four transceiver channels with multiplexing functionality. This allowed us to set up a system with split-beam transducers of ES70-7C, ES120-7C, and ES333-7C. The nominal half-power (3-dB) beamwidth of all transducers corresponds to 7°. Detailed descriptions of acoustic data collection are presented in SM3–1.

The software Echoview 9 (Echoview Software Pty. Ltd.) was used to calculate the mean volume backscatter strength S_v and to remove echoes from fish and methane bubbles rising from the bottom (see SM3–2 for more details on data pre-processing).

The pre-processed S_v values averaged over pings on 3 Apr are shown in Fig. 1a. From the three profiles we found that the drastic change in the average slopes of S_v (i.e. $\frac{\Delta S_v}{\Delta z}$) occurred at z_{ref} of 2.1 m, 1.8 m, and 0.3 m for 70 kHz, 120 kHz, and 333 kHz, respectively. A close inspection of these slopes revealed that the overall change in S_v or slope was larger at lower frequencies, indicating that at lower frequencies the scattering by *Microcystis* colonies had a stronger coherent component as well as multiple scattering, which was what one would expect since the lower the frequency, the smaller the acoustic phase difference among the adjacent scatterers, hence the stronger the scattering coherence. More specifically, since in this application the *Microcystis* VC was practically a monotonic decreasing function of depth, S_v profiles are a decreasing function of depth, or an increasing function of the decreasing distance toward the water surface. At a particular depth shallower than ~2 m, when the VC increased closer to the water surface to a level that the average distance between *Microcystis* cells was still smaller compared with the wavelength at lower frequency (smaller phase difference), such as 70 kHz, but was relatively larger than those at higher frequencies (larger phase difference), such as 120 kHz or 333 kHz, the resultant coherent scattering at 70 kHz was larger than that at higher frequencies.

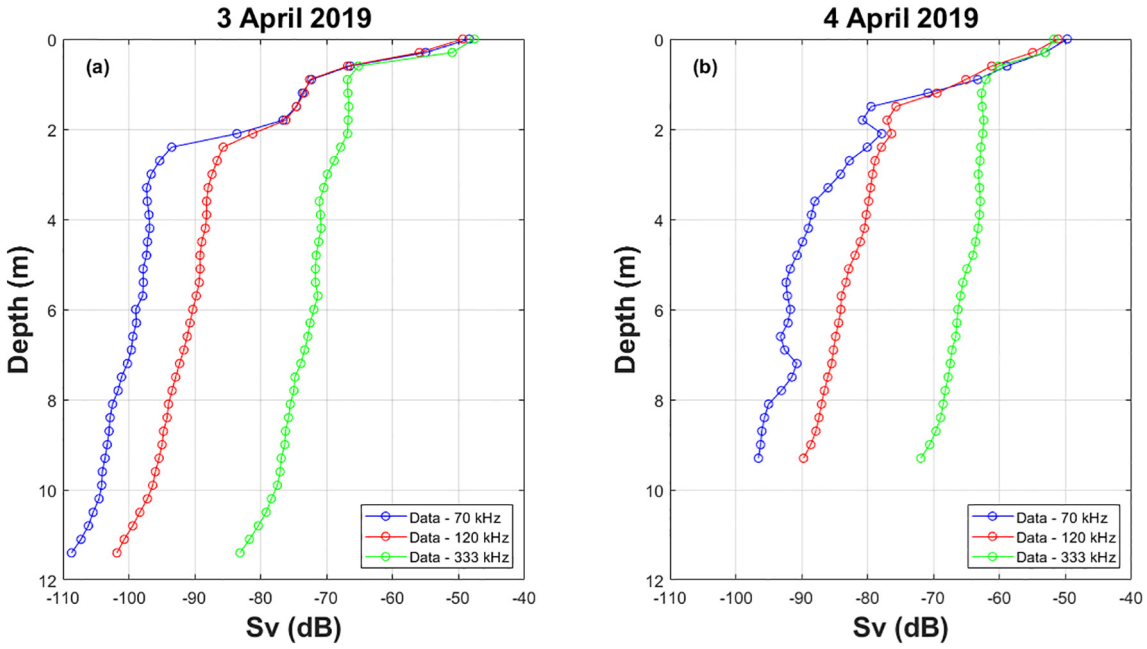

Fig. 1. The S_v vertical profiles recorded with Simrad EK80 echosounders at 70, 120, and 333 kHz on (a) 3 Apr and (b) 4 Apr 2019. The three profiles in each panel were obtained from the fish-echo removed echograms (bottom row of Figs. SM3–2a and 2b) and averaged over 26 min for 0.3 m depth bins. The profiles were measured during the bloom of gas-bearing cyanobacterium *Microcystis* sp. in Lake Kinneret and depict the acoustic backscatter responses from various layers at three ultrasonic frequencies.

2.4.2. Ground truth measurements of Microcystis colony volume concentration

In situ optical data measured with the LISST-100× were used as proxies for *Microcystis* colony volume concentrations in the water. This has been previously achieved using a laser particle analyzer (Li et al., 2014; Lin et al., 2015; Hozumi et al., 2019). Measurements with the LISST-100× correlated with microscopic results for spherical cell shapes (Karp-Boss et al., 2007) and for cells from isolated *M. aeruginosa* cultures (Andrews et al., 2010). The detailed descriptions of *Microcystis* VC measurements with LISST-100× are given in SM4.

In situ measurements of *Microcystis*-bound chlorophyll *a* (Chl a_{Micro}) concentration profiles were also carried out with a submersible spectrofluorometer probe (FluoroProbe, bbe-Moldaenke, Kiel, Germany) (see SM5 for more details on Chl a_{Micro} data acquisition).

2.5. Relation between Microcystis VC and concentration of Chl a_{Micro}

The VC data (Fig. SM4-1a) was measured only on 3 Apr 2019. In order to approximate the VC on 4 Apr 2019, which was required for the model, we associated it with Chl a_{Micro}, as a proxy of *Microcystis* biomass, since vertical profiles of concentrations of Chl a_{Micro} ($C_{\text{Chl } aMicro}$) were measured on both dates. A linear relationship between the VC and associated $C_{\text{Chl } aMicro}$ was derived from the data measured on 3 Apr 2019 (Fig. 2):

$$\text{VC}|_{\text{Apr3}} = 1.19\, C_{\text{Chl } aMicro}|_{\text{Apr3}} + 1.70, \tag{11}$$

where $C_{\text{Chl } aMicro}$ is in μg L^{-1}.

This equation allowed us to approximate the VC profile on 4 Apr 2019 based on the measured $C_{\text{Chl } aMicro}$ vertical profile. Still, using the $C_{\text{Chl } aMicro}$ regression to estimate the VC on 4 Apr 2019 might not be precise since the fluorometrically measured $C_{\text{Chl } aMicro}$ could be potentially biased near the water surface, where *Microcystis* VC was high. The reason was the chlorophyll fluorescence quenching effect at high light intensity (e.g. Cullen, 1982; Sackmann et al., 2008). To get around this problem, we assumed that the relative change in vertical profile of VC measured on 4 Apr 2019 was similar to that measured on 3 Apr since the same FluoroProbe was used for measurements in two consecutive days, such that the estimated slope in Eq. (11) obtained on 3 Apr 2019 could be also applicable to $C_{\text{Chl } aMicro}(z)$ relationship on 4 Apr:

$$\text{VC}(z)|_{\text{Apr4}} = \text{VC}(z)|_{\text{Apr3}} + 1.19\, C_{\text{Chl } aMicro}(z)\Big|_{\text{Apr3}}(R_{chl}(z) - 1), \tag{12}$$

where $R_{chl}(z) = \frac{C_{\text{Chl } aMicro}(z)|_{\text{Apr4}}}{C_{\text{Chl } aMicro}(z)|_{\text{Apr3}}}$. Note that Eq. (12) is independent of intercept term [1.70 in Eq. (11)]. Using Eq. (12) with a ratio term $R_{chl}(z)$ and $C_{\text{Chl } aMicro}(z)$ measured on 4 Apr, allowed us to extend the range of the relationship between VC and $C_{\text{Chl } aMicro}$. Since Eq. (11) was derived based on the data with lower VC and $C_{\text{Chl } aMicro}$ (VC < 20 μL L^{-1} and $C_{\text{Chl } aMicro}$ < 12 μg L^{-1}), the calculated VC near the water surface that corresponded to much larger $C_{\text{Chl } aMicro}$ than 12 μg L^{-1} and were significantly larger than 20 μL L^{-1}, may be less accurate due to fluorescence quenching. In deriving Eq. (12), we assumed that the relative changes in VC and $C_{\text{Chl } aMicro}$ were the same on both dates, i.e. the same slope of,1.19 even at ranges exceeding those used for deriving Eq. (11) but with different intercepts.

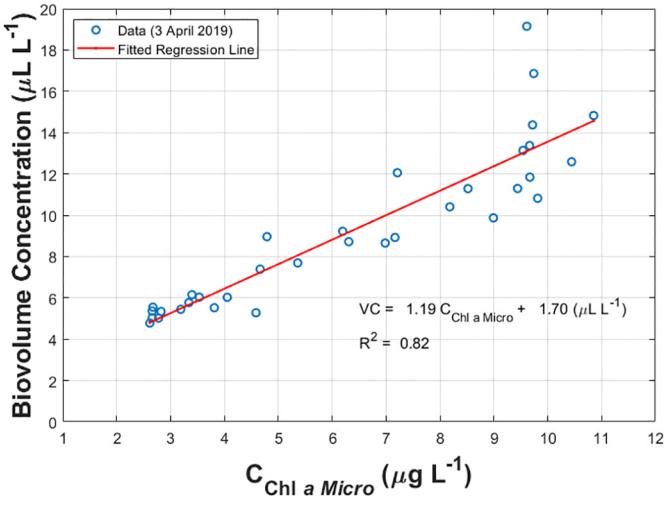

Fig. 2. Relationship between *Microcystis* volume concentration (VC) and concentration of Chl a_{Micro} ($C_{\text{Chl } aMicro}$) measured on 3 Apr 2019. The straight line is the linear regression [Eq. (11)]. The regression can be valid for the measured range of concentrations and may not be valid beyond its domain.

3. Results

3.1. Acoustic backscattering of Microcystis population at various depth and frequencies

Acoustic backscattering of *Microcystis* was modelled using Eqs. (4)–(6). The physical properties of the elastic vesicle walls of gas-bearing vesicles (shells) are shown in Table SM6–1, which are adopted directly from Walsby (1994). The other modeling parameters used to compute the acoustic backscattering of the cyanobacterium are presented in Table 1. The parameters a_0 and p_0, as well as the three z_{ref} values at three frequencies, were estimated using the non-linear least-square fit between the vertical profiles of the echosounder data and the model. The probability density function of *Microcystis* cell diameter distribution, $P_d(a_{cell})$ [Eq. (2)], was confined between 2.5 μm and 3.2 μm with 0.1 μm resolution. The measured mean diameter of *Microcystis* cells was 2.8 μm and the mean cell separation in colonies (the mean distance between cell centers in colonies) was $\bar{d}_{cell} = 3.8$ μm, hence the calculated packing factor $\phi_p = \phi_s \times \left(\frac{2\bar{a}_{cell}}{\bar{d}_{cell}}\right)^3 = 0.26$, where $\phi_s = 0.64$ is the packing factor with a randomly close-packed sphere model (Scott and Kilgour, 1969; Torquato et al., 2000).

The comparison of the vertical profiles of S_v measured in the lake on 3 Apr 2019 and modelled ones is shown in Fig. 3. The overall fit is reasonably good. The $\langle \Delta S_v \rangle$ at the three frequencies (70, 120, and 333 kHz) are −0.12, −0.06, and − 0.35 dB, respectively, the corresponding ϵ_{rms} at those frequencies are 2.07, 1.23, and 1.02 dB, respectively. The computed vertical profiles depict two features imbedded in the model [Eqs. (4)–(6)]: (1) At depths > z_{ref}, the majority of the coherent scattering stemmed from the contribution of *Microcystis* cells within colonies, a constant power term [$p_0 = 1.29$ in Eq. (5)] that is greater than unity (Table 1); (2) at shallower depths (increasing VC), in addition to the

Table 1
Acoustic modeling parameters inferred from the non-linear inverse algorithm.

Parameters	Values		Unit
	3 Apr 2019	4 Apr 2019	
a_0	0.090	0.083	dimensionless
p_0	1.29	1.31	dimensionless
ϕ_p	0.26		dimensionless
f_{ref}	120		kHz
$\langle TS(f, \bar{a}_{cell}) \rangle_{acell}$ at 70 kHz	−217.2		dB re 1 m^2
$\langle TS(f, \bar{a}_{cell}) \rangle_{acell}$ at 120 kHz	−207.9		dB re 1 m^2
$\langle TS(f, \bar{a}_{cell}) \rangle_{acell}$ at 333 kHz	−190.1		dB re 1 m^2
z_{ref} for 70 kHz	2.1	1.2	m
z_{ref} for 120 kHz	1.8	0.9	m
z_{ref} for 333 kHz	0.3	0.1	m

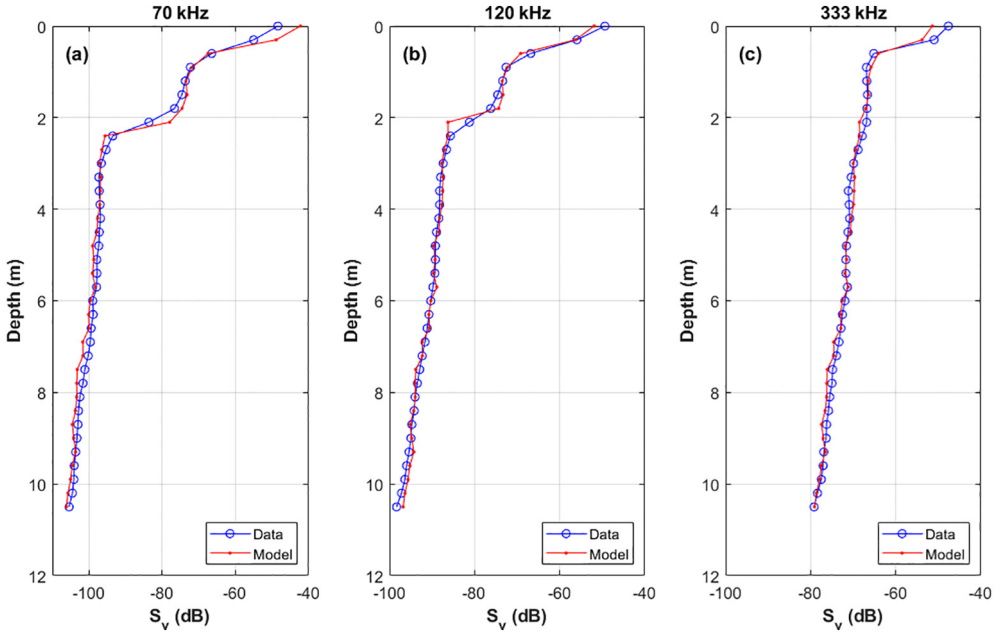

Fig. 3. The S_v vertical profiles measured with the echosounder (Data) and predicted by the model (Model) at 70, 120, and 333 kHz (3 Apr 2019). The empirically fitted model parameters in Eq. (5) are presented in Table 1.

coherent scattering from within cells, a stronger contribution from the coherent scattering resulting from inter-colony interaction apparently played an important role in characterizing the acoustic scattering of *Microcystis*. The largest values of power terms, i.e., $p(f)$, were 1.61, 1.46, and 1.32 for 70, 120, and 333 kHz, respectively.

The agreement of the model predictions using Eqs. (4)–(6) (see Table 1 for the modeling parameters) with the data collected on 4 Apr 2019 (Fig. 1b) is similar to that for 3 Apr 2019 (Fig. SM7–1). The slight difference in modeling parameters for 4 Apr and 3 Apr (Table 1) was likely due to some uncertainty in estimating the VC profile in the upper part of the water column on 4 Apr since its VC profile was calculated based on the measured $C_{\text{Chl }aMicro}$ profiles using Eq. (12) by taking into account the VC - $C_{\text{Chl }aMicro}$ relationship obtained in the previous day. The $\langle \Delta S_v \rangle$ at the three frequencies (70, 120, and 333 kHz) are −1.97, −0.28, and − 0.68 dB, respectively, and the corresponding ϵ_{rms} at the three frequencies are 2.72, 1.71, and 1.63 dB, respectively. Although we used a VC profile estimated by using Eq. (12), the data/model agreement is similar to that for 3 Apr for depths >4 m. However, the data/model agreement at depths <4 m is not as good as that for 3 Apr due to lower accuracy of the VC evaluated for 4 Apr based on $C_{\text{Chl }aMicro}$.

3.2. Biovolume concentration (VC) estimates

Quantification of the *Microcystis* VC from the acoustically measured quantity, S_v, is an inverse problem, which is opposite to the forward problems discussed above. Here we will present two inverse problem approaches to estimation of the *Microcystis* biomass concentration: one is model-based approach and the other one is an empirical solution.

3.2.1. Model-based estimate

The VC, as a function of the measured acoustic quantity, S_v, was estimated from vertical profiles of S_v. Due to the complex nature of the scattering model, the inverse problem was solved by nonlinear inversion methods (Levenberg, 1944; Menke, 2012; Chu et al., 2016; Aster et al., 2018). Since both VC and S_v were nearly a monotonic function of depth, we related both quantities directly by using the data collected on 3 Apr 2019. The inferred VC based on S_v is shown in Fig. 4. Since we were not able to measure the VC on 4 Apr, the VC values were estimated based on the measured $C_{\text{Chl }aMicro}$ using Eq. (12) as described above. The measured and predicted values agreed reasonably well, especially at the higher biovolume concentrations measured at larger S_v values close to the water surface (Fig. SM8–1).

3.2.2. Empirical regression estimate

Although Eqs. (4)–(6) establish a partially coherent relation between the VC and the observed S_v, the inverse problem of converting S_v to VC is a complex task for modeling. An alternative way to resolve this inverse problem is to use a purely empirical approach by correlating these variables.

However, it can be helpful if we examine the forward problem using the empirical approach first, where the backscattering quantity, S_v, is expressed as a function of VC in the logarithmic domain ($\log_{10}$VC). The later approach has been implemented by Ostrovsky et al. (2020), where the relationship between the S_v and logVC was approximated

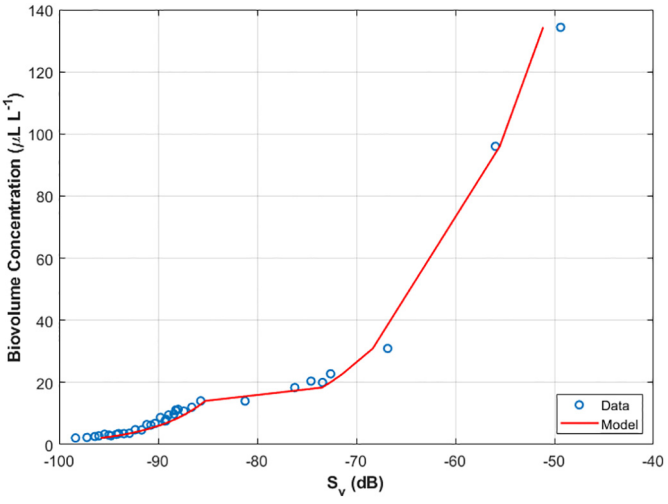

Fig. 4. Estimates of model-based adjusted *Microcystis* biovolume concentration (VC) as a function of mean volume backscattering strength (S_v) at 120 kHz (3 Apr 2019). The theoretical curve (solid red line) allows assessing the mean biovolume concentration profiles as a function of depth, as VC decreases monotonically with depth and S_v. The open circles are the measured values.

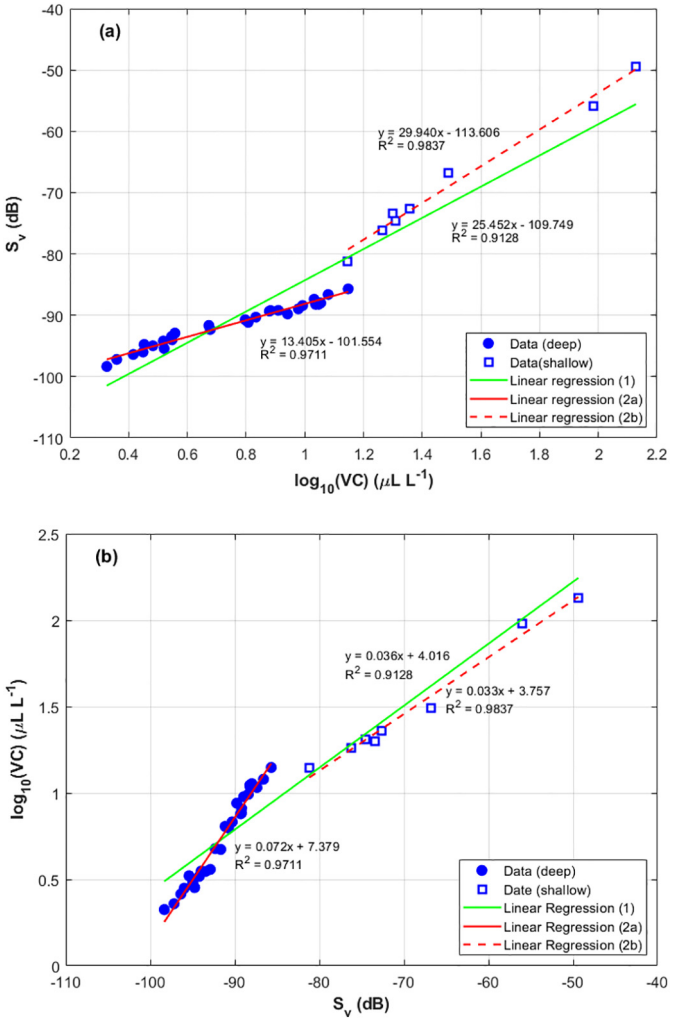

Fig. 5. Relationships between volume backscatter strength (S_v) at 120 kHz and *Microcystis* volume concentration (VC) at different depth ranges on 3 Apr 2019. The filled blue circles represent the data collected at depths >2 m (regression line is shown by red solid line); the empty blue squares represent the measurements collected at depths <2 m (regression line is shown by red dashed line). The green solid line is the linear regression for all data. The vertical profiles of S_v at 120 kHz is shown in Fig. 1a (red circles) and the VC profile is given in Fig. SM4-1a. (a) S_v as a function of $\log_{10}$(VC); (b) $\log_{10}$(VC) as a function of S_v.

by a linear regression line. Using such an approach for the entire data set (0 to 11 m depth) collected at 120 kHz on 3 Apr 2019, $S_v = 25.5\log_{10}\mathrm{VC} - 109.7$ (Fig. 5a, green line). A more careful inspection of the data reveals that the measured data can be much better approximated by two separate regressions corresponding to the S_v regions below −85 dB (filled circles) and above −85 dB (empty squares). The threshold of −85 dB corresponds to the depth of about 2 m (cf. z_{ref} in Table 1), which separates the two scattering regions (Figs. 1 and 3). The corresponding linear regression lines computed separately for the two regions are shown by two red lines (Fig. 5a).

Similarly, we can solve the inverse problem using a simple linear regression by switching the X-axis ($\log_{10}$VC) and Y-axis (S_v), as

$$\log_{10}\mathrm{VC} = kS_v + C \tag{13}$$

where k and C are slope and intercept of the linear regression in log-log domain of VC (μL L^{-1}) and s_V.

The results of using empirical linear-regression approach for all three frequencies from the data collected on 3 Apr 2019 are summarized in Table SM9–1 where the fitted regression parameters by using both a single linear regression for the entire data and two linear regression lines for the deep and shallow strata are provided. It is observed that at 70 kHz (Fig. 3a), when $S_v > -94$ *dB*, the VC increases significantly faster in the shallower layer closer to the surface. Such increases are also observed for 120 and 333 kHz, with the S_v thresholds of around −85 *dB* (Fig. 3b), and−75 *dB* (Fig. 3c), respectively. In this shallower layer that is very close to the water surface, the measured VCs of *Microcystis* were very high (> 50 μL L^{-1}, Fig. SM4-1a).

3.3. Estimate of the areal volume concentration

Comparison of the AVC of *Microcystis* calculated using the scattering model-based and empirical regression-based approaches using acoustic measurements at 120 kHz at two sampling dates is presented here to demonstrate the capability of the models.

For scattering model-based approach, the AVCs (mL m^{-2}) were calculated by integrating the VC (μL L^{-1}) over the sampled column (~10-m thick). Then, we used the measured vertical S_v profiles (Fig. 1) for calculation of the AVC based on the acoustic backscattering model approach (Fig. 4). The model-based estimates of the AVC were 165 mL m^{-2} and 139 mL m^{-2} for 3 Apr and 4 Apr 2019, respectively. The relative differences from the measured biovolumes were 1.9% and 2.2%, respectively (Table 2). Note that the measured VC on Apr 4 was estimated indirectly by Eq. (12) based on fluorometric measurements of Chl *a* vertical profile, which could introduce some uncertainty in the VC estimate in shallow depths (see below). Thus, the resultant scattering model predictions provide a reasonable agreement with the measured *Microcystis* biomass proxies.

For regression-based approach, the empirical linear regression method [Eq. (13)] was implemented to estimate the *Microcystis* AVC. This method was used in two modifications: (1) one regression was used to the entire acoustically sampled depth range and (2) two separate depth-specific regressions were implemented to shallow (<2-m) and deeper (>2-m depth) sections of the water column (Fig. 5b). The single regression line approach resulted in AVCs of 164 mL m^{-2} and 134 mL m^{-2} for 3 Apr and 4 Apr 2019, respectively. The relative differences from the measured biovolumes were 1.4% and − 1.2%, respectively. The use of two separate regressions for two depth ranges resulted in AVCs of 160 mL m^{-2} and 134 mL m^{-2} for 3 Apr and 4 Apr 2019, respectively. The relative differences from the measured biovolumes were − 1.2% and − 0.5%, respectively. A summary of the AVC estimates is presented in Table 2.

4. Discussion

4.1. Acoustic backscattering of Microcystis

The proposed physics-based scattering model [Eqs. (4) and (5)] are based on the five assumptions given in Section 2.2. These assumptions are introduced to simplify the complex mechanisms of acoustic scattering by densely aggregated *Microcystis* colonies. As a result, some floating parameters ($a_0, p_0, \phi_p, z_{ref}$) in the scattering model are used to fit the acoustic data.

The dependence of z_{ref} on echosounder frequency (Fig. 3 and Table 1) is believed resulted from the inherent constructive and destructive nature of acoustic scattering among *Microcystis* cells. When the mean phase difference, $\langle\Delta\phi\rangle = k\bar{d}$ is small (should not confuse the $\Delta\phi$ with the packing factor, ϕ_p), i.e., $\Delta\phi \ll \pi$, where $k = 2\pi/\lambda$ is the acoustic wave number, λ is the acoustic wavelength, and $\bar{d}$ is the average distance between cells (either intra- or inter-colonies), the contributions of acoustic scattering from the adjacent cells are coherently added, otherwise the contributions could be constructive or destructive depending on $\langle\Delta\phi\rangle$. For a given value of $\bar{d}$, which was associated to a certain VC, the $\langle\Delta\phi\rangle$ depended only on acoustic frequency. At lower frequency, stronger scattering coherence among *Microcystis* cells

Table 2
Comparison of the areal volume concentration (AVC) of *Microcystis* calculated using the model-based and empirical regression-based methods using the acoustic measurements at 120 kHz at two sampling dates. Two empirical regression approaches are used for AVC calculations: (1) one-regression is calculated for the entire water column, and (2) two depth-specific regressions are calculated for the shallow (<2-m) and deep (>2-m depth) strata (Fig. 5b). Relative differences from the measured AVC for all three methods are presented.

Date	Measured/inferred AVC (mL m^{-2})	Computed AVC (mL m^{-2})	Relative difference	Computation method
3 Apr 2019	162	165	1.9%	Model-based
		164	1.4%	One-regression approach (1)
		160	−1.2%	Two-regressions approach (2)
4 Apr 2019	136	139	2.2%	Model-based
		134	−1.2%	One-regression approach (1)
		134	−0.5%	Two-regressions approach (2)

occurred at lower VC (larger $\overline{d}$). In our case the VC was a monotonically decreasing function of depth, i.e. lower VC was characteristic for deeper depths. As a result, at lower frequency, smaller VC (occurring in deeper locations) should be responsible for stronger scattering contributions from *Microcystis* cells possessing higher coherence.

As mentioned in Section 3.1, both $\langle \Delta S_v \rangle$ and ϵ_{rms} from 4 Apr 2019 are noticeably larger than those from 3 Apr 2019 resulting from less accurate data/model S_v profile fits near the surface. This is not surprising since the VC inferred from Eq. (12) could be less accurate because of quenching of Chl *a* fluorescence, as discussed above (Section 2.5). Despite the larger mismatch and small difference in fitting parameters, the scattering model still capture the general trends of the measured data (Fig. SM7–1), suggesting the model be useful, especially the deeper range where VC values are low. Nevertheless, direct in-situ estimating the VC (e.g. with LISST-100×) is important for proper assessment of the *Microcystis* biomass and accurate modeling of its acoustic properties.

Although the current model is not able to provide a more rigorous quantitative description of this "coherent scattering" from both inner- and inter-colony interactions, as well as the multiple scattering among the cells and colonies, it uses a semi-empirical power term, Eq. (5), to depict the complicated scattering mechanisms.

Note that since the vesicles, or modelled spherical shells, were very small, the dimensionless quantity, $ka_s \ll 1$, and even below the resonance frequency of the equivalent thin elastic spherical shell, the scattering was in the Rayleigh scattering region. When depth was deeper than 2 m (less coherent due to lower VC at deeper locations, see Fig. 1), the backscattering cross section was proportional to the 4th power of frequency, i.e. $\sigma_{bs} \propto f^4$ (Rayleigh, 1899; Clay and Medwin, 1977). By careful inspection of Fig. 1, we found that at depths >2 m the S_v value differences between the three frequencies remained broadly constant. For instance, at 6 m, the difference between 120 and 70 kHz was approximately 8.1 dB and between 333 and 70 kHz was approximately 27.5 dB. These were close to the theoretical predictions:

$$\Delta S_{v120-70} = S_v(120\ \text{kHz}) - S_v(70\ \text{kHz}) = 40 \log_{10} \frac{120}{70} \approx 9.4\ \text{dB} \quad (14)$$

and

$$\Delta S_{v333-70} = S_v(333\ \text{kHz}) - S_v(70\ \text{kHz}) = 40 \log_{10} \frac{333}{70} \approx 27.1\ \text{dB} \quad (15)$$

The small mismatches might result from the uncertainties in predicting the weak frequency-dependent coherent scattering (p_0 slightly greater than unity, see Table 1) and/or some uncertainty of measuring VC by LISST in the upper slightly stratified water layer. With the increase in VCs, the frequency-dependent coherent scattering became more important. At shallow near-surface depths, the VC was high and the backscattering at all three frequencies increased fast toward the water surface and became very high, reaching about −50 dB for all three frequencies, and $\Delta S_{v120-70}$ and $\Delta S_{v333-70}$ were no longer following $\sigma_{bs} \propto f^4$ and display more complex relationship.

Although we were not able to develop a rigorous scattering model yet, our partially coherent scattering model generally captured the overall scattering pattern and depicted the frequency and depth dependences. This can help revealing the important scattering patterns that are inherently associated with the acoustic properties of cyanobacterium *Microcystis*.

4.2. Biovolume concentration (VC) estimates

4.2.1. Model-based estimate

Although depth is not directly shown in Fig. 4, it should be kept in mind that both S_v and VC increase monotonically toward the water surface (Fig. 1 and Fig. SM4-1a). The fact that the larger S_v values resulting from higher VC were observed at shallow depths has a crucial importance for quantification of the buoyant toxic cyanobacteria, as the biomass in the upper 2-m stratum (around and above the diurnal thermocline) contributed about 65% of the total biomass over the investigated upper 10-m water column. It was also observed that concurrently with the increase in *Microcystis* VC toward the water surface, the concentration of large *Microcystis* colonies also enlarged (Fig. SM4-1c). The influence of this variable on the acoustic backscatter was not considered directly in the current model, but implicitly such an impact was included by varying power term $p(f,z)$ defined in Eq. (5). The acoustic properties of the *Microcystis* population with complex colony size distribution and varying density over depth and locations should be further investigated and be a subject of model development.

4.2.2. Empirical regression estimate

It is well known that for a completely incoherent scattering scenario, the theoretical slope of S_v vs. $\log_{10}$VC is 10 (Knudsen, 1990). Practically the same slope of 9.9 of S_v vs. $\log_{10}$Chl *a* was reported for *Microcystis* by Ostrovsky et al. (2020) in the controlled tank experiment. In Lake Kinneret a slightly higher slope of 13.4 was characteristic for the regression line in the region with low S_v values (> 2 m) (Fig. 5a). Similar slope of 12.8 was also detected by Ostrovsky et al. (2020) in Lake Dianchi (China). Such slopes indicate a scattering mechanism of weak coherence. They are also close to the parameter of the acoustic scattering model of $p = p_0 = 1.29$ (Table 1, constant power term in Eq. (5)), which leads to a slope of $\approx 10p_0 = 12.9$. In the shallowest depth region (<2 m) of Lake Kinneret characterized by very high S_v values, the slope was about 30 (i.e. much larger than 10) that indicates a much stronger coherent scattering (the maximum power term $p \approx 1.5$ in Eq. (5)). Since the highest *Microcystis* biomass is often concentrated in the upper part of the water column, the accurate assessment of the linear regression for the near-surface layer should have large importance for accurate assessment of the integrated (areal) biomass than that for the deeper layers, where VCs are usually much lower (Ostrovsky et al., 2020).

4.3. Estimate of the areal volume concentration

While in our examples the scattering-based model [Eqs. (4)–(6)] and the empirical (linear regression) models produced rather similar results, they have different advantages and disadvantages. The scattering model presented here was heuristic with a few floating parameters that were determined based on the least-square model/data

comparison (Table 1). The model results were based on the five assumptions outlined in the Section 2.2, which are difficult to estimate quantitatively.

The scattering-based model takes into account the coherent scattering of the echo-reflecting objects, such as gas vesicles and *Microcystis* cells and provides a theoretical basis for quantifying the *Microcystis* biomass using the data acquired with a scientific echosounder. This is an important step forward to the development of scattering theory for the complexly packed echo-reflecting objects (vesicles ➔ cells ➔ colonies) of different densities. The current scattering model is unable to take into account the influence of varying colony size distribution, as it depicts only the total biovolume (VC), i.e. the model-predicted backscatter depends only on VC, even if colony size distribution would affect the acoustic backscattering strength. Thus, the suggested modeling method is based on a semi-empirical approach that needs to be further developed and parametrized for a more rigorous scattering model. The resultant model predictions provide a reasonable agreement with the measured *Microcystis* biomass proxies (Table 2). On 3 Apr 2019 the relative difference between the scattering model-calculated AVC and AVC measured directly using VC profile was <2.0%. On 4 Apr 2019 the relative difference between the model-calculated AVC and AVC inferred from the Chl *a* profile was ~2.5%.

The empirical regression models may have good statistical ground for revealing the general relationships between the backscattering signal and biomass of the organisms and allow fast quantification of the *Microcystis* biomass in various water bodies. The occurrence of high correlations between S_v and $\log_{10}$VC in the two (shallow and deep) strata well depicts the depth-associated relationships and, thus, characterizes the essential difference in acoustic backscattering properties of *Microcystis* colonies in these strata. The latter implies importance of better understanding of the inherent nature of the scattering properties of this organism. The two-regression approach has a good potential to achieve accurate results in terms of model-data comparison (Table 2). One should note that this approach is acoustic-frequency dependent and the regression coefficients can be different for various frequencies. Computation of the using one $\log_{10}\mathrm{VC} - S_v$ regression only for the entire sampling stratum may help to evaluate roughly the AVC in the water body, where the vertical distribution of *Microcystis* is more uniform, as it was observed by Ostrovsky et al. (2020). However in our case, implementation of only one regression (Fig. 5b, green line) apparently ignores the vertical change in the relationship between $\log_{10}$VC and S_v. Also, the accuracy of the last approach for assessment of the AVC should depend on thickness of the sampled vertical stratum and, therefore, it should be used with caution.

4.4. Uncertainty of in-situ measurements of Microcystis biovolume concentrations

Assessment of the AVC (a proxy for areal biomass) of buoyant toxic cyanobacteria is a very important but challenging task. Uncertainties are inevitably involved in data collection, processing, and interpretation of the relationships between S_v and biomass in different models. One of the complexities arises from the fact that cyanobacterium *Microcystis* were mixed with fish, gas bubbles (Ostrovsky et al., 2020), and other possibly unidentified aquatic organisms (Fig. SM3–2). Inaccurately removing their strong backscattering contribution might potentially introduce a biased quantification of the backscattering signal from the *Microcystis* colonies. However, due to the distinct difference in acoustic signatures between such targets and *Microcystis*, i.e. their large contrast in S_v (Fig. SM3–2), this kind of uncertainty should be insignificant.

Estimating cyanobacterial biovolume concentration using fluorometrically measured Chl *a* using Eq. (12) could be potentially biased due to fluorometric signal quenching at high light intensity (Cullen, 1982; Sackmann et al., 2008). However, this factor did not seem to affect the biovolume data measured on 4 Apr 2019 at relatively low winter irradiance as supported by a reasonable agreement between the measurements and the modelled results (Fig. SM7–1).

Although the unbiased VC measurements with the LISST was also confirmed by high correlation between VC and $C_{\mathrm{Chl}\ aMicro}$- the two proxies of *Microcystis* biomass [Eq. (11)], it is possible that biovolume assessment using LISST-100× might also be potentially biased in a stratum of high thermal stratification (usually at the depths of the seasonal thermocline), which may lead to erroneous estimates of biovolume of large particles due to the influence of Schlieren on in-situ optical measurements (Tao and Hill, 2017; Tao, 2019). Nonetheless, during our measurements the highest buoyancy frequency (N), indicating the vertical water density stratification, hardly approached 0.035–0.05 s^{-1} above which the Schlieren would influence the optical data (Tao and Hill, 2017).

5. Conclusions

Commercially available scientific echosounders can reliably measure S_v with vertically oriented transducers in both stratified and non-stratified waters that allows quantifying the gas-bearing cyanobacteria and their vertical and lateral heterogeneity. This should greatly facilitate the ecologically important studies on the effect of ambient factors on blooming of harmful gas-bearing cyanobacteria. The acoustic model presented in this study is based on a heuristic and empirical approach assuming that the scattering from the cyanobacterium *Microcystis* is neither completely coherent nor completely incoherent. A power term, $p(f,z)$ given by Eqs. (4) and (5) was used to describe the complex scattering mechanism. The empirical fit of this power term allows quantifying the changes of multiple scattering with depth, better evaluating the *Microcystis* backscattering properties, and assessing the vertical profiles of the VC, which is a good proxy of the *Microcystis* biomass. The in-situ measured VC profiles (e.g. with LISST-100×) provide a robust basis for accurate modeling of *Microcystis* acoustic properties. The relationship between VC and $C_{\mathrm{Chl}\ aMicro}$ may not always be estimated reliably using fluorometric technique, especially in the near-surface stratum due to signal quenching at high light intensity. For *Microcystis* colonies commonly concentrated in the uppermost stratum, such a limitation can bias the AVC assessment. Empirical models, based on either a single linear regression or two linear depth-associated regressions between the S_v and the $\log_{10}$VC is also investigated. Although both types of models produce similar assessments of AVC, the scattering model provides an explicit dependence on frequency and *Microcystis* VC and can describe the backscattering signal measured with echosounder reasonably well, while the empirical models, despite of their potential to achieve even better fits to the measured data, can be case specific and possibly less flexible in applying to the acoustic data at different frequencies at high concentrations. This acoustic tool will be invaluable to effectively monitor population dynamics of toxic gas-bearing cyanobacteria, which should help to study their spatiotemporal dynamics and protect the health of human, animals, and entire aquatic ecosystems.

Author declaration

Authors declare that

1. All authors have seen and approved the final version of the manuscript being submitted
2. The article is the authors' original work, hasn't received prior publication and isn't under consideration for publication elsewhere
3. There is no conflict of interest that involves any conditions in which professional judgment concerning a primary interest, such as the validity of research, may be influenced by a secondary interest, such as financial gain
4. there's no financial/personal interest or belief that could affect our objectivity
5. The research work reported in the manuscript was partially funded by Japan-Israel cooperative scientific research program, the Ministry of Science and Technology, grant number 3–14952

6. The authors have received permission from the American Society of Microbiology to reuse a figure (Fig. 1a in the submitted manuscript) in a previously published paper (see the attached permission, https://s100.copyright.com/CustomerAdmin/PLF.jsp?ref=f2480778-28fc-4921-a0ab-65f404696e0b)

CRediT authorship contribution statement

Dezhang Chu: Conceptualization, Methodology, Validation, Formal analysis, Writing – original draft, Writing – review & editing. **Ilia Ostrovsky:** Conceptualization, Methodology, Validation, Formal analysis, Investigation, Resources, Data curation, Writing – original draft, Writing – review & editing, Project administration, Funding acquisition. **Hikaru Homma:** Formal analysis, Investigation, Data curation, Writing – review & editing.

Declaration of competing interest

The authors declare that they have no known competing financial interests or personal relationships that could have appeared to influence the work reported in this paper.

Acknowledgements

We thank Semion Kaganovsky for organization and technical support of our field measurements. We also thank the anonymous reviewers for their critical comments that have notably improved the manuscript. This work was supported by Japan-Israel Cooperative Scientific Research Program, the Ministry of Science and Technology, grant number 3-14952.

Appendix A. Supplementary data

Supplementary data to this article can be found online at https://doi.org/10.1016/j.scitotenv.2021.148573.

References

Akkermans, E., Wolf, P.E., Maynard, R., 1986. Coherent backscattering of light by disordered media: analysis of the peak line shape. Phys. Rev. Lett. 56 (14), 1471–1474. https://doi.org/10.1103/PhysRevLett.56.1471.

Andrews, S., Nover, D., Schladow, S.G., 2010. Using laser diffraction data to obtain accurate particle size distributions: the role of particle composition. Limnol. Oceanogr. Methods 8, 507–526. https://doi.org/10.4319/lom.2010.8.507.

Aster, R., Borchers, B., Thurber, Cl, 2018. Parameter Estimation and Inverse Problems. 3rd ed. Elsevier (ISBN 9780128134238).

Cherin, E., Melis, J.M., Bourdeau, R.W., Yin, M., Kochmann, D.M., Foster, F.S., Shapiro, M.G., 2016. Acoustic behavior of *Halobacterium salinarum* gas vesicles in the high frequency range: experiments and modeling. Ultrasound Med. Biol. 43, 1016–1030. https://doi.org/10.1016/j.ultrasmedbio.2016.12.020.

Chu, D., Wiebe, P.H., Lawson, G.L., Copley, N.J., 2016. Estimation of size, orientation, and abundance of marine organisms using acoustic scattering model-based inversions. J. Acoust. Soc. Am. 139, 2885–2895. https://doi.org/10.1121/1.4948759.

Clark, J.M., Schaeffer, B.A., Darling, J.A., Urquhart, E.A., Johnston, J.M., Ignatius, A.R., Myer, M.H., Loftin, K.A., Werdell, P.J., Stumpf, Richard P., 2017. Satellite monitoring of cyanobacterial harmful algal bloom frequency in recreational waters and drinking water sources. Ecol. Indic. 80, 84–95. https://doi.org/10.1016/j.ecolind.2017.04.046.

Clay, C.S., Medwin, H., 1977. Acoustic Oceanography: Principles and Applications. John Wiley & Sons, p. 544.

Codd, G.A., Lindsay, J., Young, F.M., Morrison, L.F., Metcalf, J.S., 2005. Harmful cyanobacteria: from mass mortalities to management measures. In: Huisman, J., Matthijs, H.C.P., Viesser, P.M. (Eds.), Harmful Cyanobacteria. Springer, Netherlands, pp. 1–23.

Colton, D., Kress, R., 2019. Inverse acoustic and electromagnetic scattering theory. Applied Mathematical Sciences, 4th ed. vol. 93. Springer (ISBN-13: 978-3030303501).

Cullen, J.J., 1982. The deep chlorophyll maximum: comparing vertical profiles of chlorophyll a. Can. J. Fish. Aquat. Sci. 39, 791–803. https://doi.org/10.1139/f82-108.

Godlewska, M., Balk, H., Kaczkowski, Z., Jurczak, T., Izydorczyk, K., Długoszewski, B., Jaskulska, A., Gągała-Borowska, I., Mankiewicz-Boczek, J., 2018. Night fish avoidance of *Microcystis* bloom revealed by simultaneous hydroacoustic measurements of both organisms. Fish. Res. 207, 74–84. https://doi.org/10.1016/j.fishres.2018.05.025.

Goodman, R.R., Stern, R., 1962. Reflection and transmission of sound by elastic spherical shells. J. Acoust. Soc. Am. 34, 3252–3267. https://doi.org/10.1121/1.1928120.

Gordon, W., 1958. Incoherent scattering of radio waves by free electrons with applications to space exploration by radar. Proc. IRE 46 (11), 1824–1829. https://doi.org/10.1109/JRPROC.1958.286852.

Hahn, T.R., 2007. Low frequency sound scattering from spherical assemblages of bubbles using effective medium theory. J. Acoust. Soc. Am. 122, 236–253. https://doi.org/10.1121/1.2793610.

Hofmann, H., Peeters, F., 2013. *In-situ* optical and acoustical measurements of the buoyant cyanobacterium *P. Rubescens*: spatial and temporal distribution patterns. PLoS One 8 (11), e80913. https://doi.org/10.1371/journal.pone.0080913.

Hozumi, A., Ostrovsky, I., Sukenik, A., Gildor, H., 2019. Turbulence regulation of Microcystis surface scum formation and dispersion during a cyanobacteria bloom event. Inland Waters 10 (1), 51–70. https://doi.org/10.1080/20442041.2019.1637681.

Huber, A.M.R., Peeters, F., Lorke, A., 2011. Active and passive vertical motion of zooplankton in a lake. Limnol. Oceanogr. 56 (2), 695–706. https://doi.org/10.4319/lo.2011.56.2.0695.

Huisman, J., Hulot, F.D., 2005. Population dynamics of harmful cyanobacteria. In: Huisman, J., Matthijs, H.C.P., Viesser, P.M. (Eds.), Harmful Cyanobacteria. Springer, Netherlands, pp. 143–176 https://doi.org/10.1007/1-4020-3022-3_7.

Ishimaru, A., 1978. Wave Propagation and Scattering in Random Media. Academic, New York https://doi.org/10.1016/C2013-0-10906-3.

Kargl, S.G., Marston, P.L., 1989. Observations and modeling of the backscattering of short tone bursts from a spherical shell: lamb wave echoes, glory, and axial reverberations. J. Acoust. Soc. Am. 85, 1014–1028. https://doi.org/10.1121/1.397485.

Karp-Boss, L., Azevedo, L., Boss, E., 2007. LISST-100 measurements of phytoplankton size distribution: evaluation of the effects of cell shape. Limnol. Oceanogr. Methods 5 (11), 396–406. https://doi.org/10.4319/lom.2007.5.396.

Kim, H., Kang, D., Jung, S.W., 2018. Development and application of an acoustic system for harmful algal blooms (HABs, red tide) detection using an ultrasonic digital sensor. Ocean Sci. J. 53, 91–99. https://doi.org/10.1007/s1260-017-0061-0.

Knudsen, H., 1990. The Bergen Echo integrator: an introduction. ICES J. Mar. Sci. 47, 167–174. https://doi.org/10.1093/icesjms/47.2.167.

Kouzoubov, A., 2018. Multiple scattering effect in acoustic response from a bubble. Proc. ACOUSTICS 2018. Nov. Adelaide, Australia, pp. 7–9.

Lavery, A.C., Chu, D., Moum, J.N., 2010. Measurements of acoustic scattering from zooplankton and oceanic microstructure using a broadband echosounder. ICES J. Mar. Sci. 67, 379–394. https://doi.org/10.1093/icesjms/fsp242.

Levenberg, K., 1944. A method for the solution of certain nonlinear problems in least squares. Qtr. Appl. Math. 2, 164–168. https://doi.org/10.1090/qam/10666.

Li, M., Zhu, W., Gao, L., 2014. Analysis of cell concentration, volume concentration, and colony size of Microcystis via laser particle analyzer. Environ. Manag. 53, 947–958. https://doi.org/10.1080/02705060.2014.976666.

Lin, L., Appiah-sefah, G., Li, M., 2015. Using a laser particle analyzer to demonstrate relationships between wind strength and Microcystis colony size distribution in Lake Taihu, China. J. Freshw. Ecol. 30 (3), 425–433. https://doi.org/10.1080/02705060.2014.976666.

Lorke, A., McGinnis, D.F., Spaak, P., Wüest, A., 2004. Acoustic observations of zooplankton in lakes using a Doppler current profiler. Freshw. Biol. 49 (10), 1280–1292. https://doi.org/10.1111/j.1365-2427.2004.01267.x.

Markensten, H., Moore, K., Persson, I., 2010. Simulated lake phytoplankton composition shifts toward cyanobacteria dominance in a future warmer climate. Ecol. Appl. 20 (3), 752–767. https://doi.org/10.1890/08-2109.1.

Martin, L.V., Stanton, T.K., Wiebe, P.H., Lynch, J.F., 1996. Acoustic classification of zooplankton. ICES J. Mar. Sci. 53, 217–224. https://doi.org/10.1006/jmsc.1996.0025.

Menke, W., 2012. Geophysical Data Analysis: Discrete Inverse Theory. 3rd ed. Academic Press, Inc., New York https://doi.org/10.1016/B978-0-12-397160-9.00001-1 293 pp.

Mishra, S., Stumpf, R.P., Schaeffer, B.A., et al., 2019. Measurement of cyanobacterial bloom magnitude using satellite remote sensing. Sci. Rep. 9, 18310. https://doi.org/10.1038/s41598-019-54453-y.

Morse, P.M., Ingard, K.U., 1986. Theoretical Acoustics. Princeton Univ. Press, Princeton, NJ (ISBN 0-691-08425-4).

Ostrovsky, I., 2003. Methane bubbles in Lake Kinneret: quantification and temporal and spatial heterogeneity. Limnol. Oceanogr. 48 (3), 1030–1036. https://doi.org/10.4319/lo.2003.48.3.1030.

Ostrovsky, I., McGinnis, D.F., Lapidus, L., Eckert, W., 2008. Quantifying gas ebullition with echosounder: the role of methane transport by bubbles in a medium-sized lake. Limnol. Oceanogr. Methods 6, 105–118. https://doi.org/10.4319/lom.2008.6.105.

Ostrovsky, I.S., Sukenik, A., Yacobi, Y.Z., Katsnelson, B., Uzhanskii, E., Moses, W.J., 2017. Hydroacoustic assessment of spatiotemporal dynamics of toxic cyanobacteria *Microcystis*: The role of physical factors in bloom formation. 4th Underwater Acoustics Conference and Exhibition, 3–8 Sep., Greek Island of Skiathos, Greece.

Ostrovsky, I.S., Uzhanskii, E., Kaganovsky, S., Katsnelson, B., 2018. Implementation of acoustic methodology for investigation of the ecology of gas-containing toxic Cyanobacterium *Microcystis* sp. Proc. Joint Conf. Acoust., 11–14 Sep., IEEE Xplore https://doi.org/10.1109/ACOUSTICS.2018.8502288.

Ostrovsky, I., Wu, S., Li, L., Song, L., 2020. Bloom-forming toxic cyanobacterium Microcystis: quantification and monitoring with a high-frequency echosounder. Water Res. 183, 1–13. https://doi.org/10.1016/j.watres.2020.116091.

Paerl, H.W., Paul, V.J., 2012. Climate change: links to global expansion of harmful cyanobacteria. Water Res. 46 (5), 1349–1363. https://doi.org/10.1016/j.watres.2011.08.002.

Park, J., Kim, K.W., 2017. Microscopy of microbial gas vesicles. Appl. Microsc. 47 (3), 165–170. https://doi.org/10.9729/AM.2017.47.3.165.

Pfeifer, F., 2012. Distribution, formation and regulation of gas vesicles. Nat. Rev. Microbiol. 705–715 (2012), 10. https://doi.org/10.1038/nrmicro2834.

Pobel, D., Robin, J., Humbert, J.-F., 2011. Influence of sampling strategies on the monitoring of cyanobacteria in shallow lakes: lessons from a case study in France. Water Res. 45 (3), 1005–1014. https://doi.org/10.1016/j.watres.2010.10.011.

Potiris, E., Frangoulis, C., Kalampokis, A., Ntoumas, M., Pettas, M., Petihakis, G., Zervakis, V., 2018. Acoustic Doppler current profiler observations of migration patterns of zooplankton in the Cretan Sea. Ocean Sci. 14 (5). https://doi.org/10.5194/os-14-783-2018.

Rayleigh, Lord, 1899. XXXIV. On the transmission of light through an atmosphere containing small particles in suspension, and on the origin of the blue of the sky. The London, Edinburgh, and Dublin Philosophical Magazine and Journal of Science. 47(287), pp. 375–384. https://doi.org/10.1080/14786449908621276.

Reynolds, C.S., Oliver, R.L., Walsby, A.E., 1987. Cyanobacterial dominance: the role of buoyancy regulation in dynamic lake environments in dynamic lake environments. N. Z. J. Mar. Freshw. Res. 21 (3), 379–390. https://doi.org/10.1080/00288330.1987.9516234.

Sackmann, B., Perry, M., Eriksen, C., 2008. Seaglider observations of variability in daytime fluorescence quenching of chlorophyll-a in northeastern Pacific coastal waters. Biogeosci. Discuss. 5, 2839–2865. https://doi.org/10.5194/bgd-5-2839-2008.

Scott, G.D., Kilgour, D.M., 1969. The density of random close packing of spheres. Brit. J. Appl. Phys. 2, 863–866.

Simmonds, J., MacLennan, D., 2005. Fisheries acoustics. Theory Pract., 20–69 https://doi.org/10.1002/9780470995303.

Stanton, T.K., Wiebe, P.H., Chu, D., Benfield, M.C., Scanlon, L., Martin, L., Eastwood, R.L., 1994. On acoustic estimates of zooplankton biomass. ICES J. Mar. Sci. 51, 505–512. https://doi.org/10.1006/jmsc.1994.1051.

Stanton, T.K., Chu, D., Wiebe, P.H., 1998. Sound scattering by several zooplankton groups. II. Scattering models. J. Acoust. Soc. Am. 103, 236–253. https://doi.org/10.1121/1.421110.

Tao, J., 2019. Characterization of Estuarine Particle Dynamics Using Optical Properties. Ph. D Dissertation. Dalhousie University, Halifax, Nova Scotia, Canada.

Tao, J., Hill, P.S., 2017. Evaluation of optical proxies for suspended particulate mass in stratified waters. J. Atmos. Ocean. Technol. 34, 2203–2212. https://doi.org/10.1175/JTECH-D-17-0042.1.

Torquato, S., Truskett, T.M., Debenedetti, P.G., 2000. Is random close packing of spheres well defined? Phys. Rev. Lett. 84, 2064–2067. https://doi.org/10.1103/PhysRevLett.84.2064.

Walsby, A.E., 1994. Gas Vescles. Microbiol. Mol. Biol. Rev. 58, 94–144.

Yang, Y., Qiu, Z., Hou, X., Sun, L., 2017. Ultrasonic characteristics and cellular properties of anabaena gas vesicles. Ultrasound Med. Biol. 43 (12), 2862–2870. https://doi.org/10.1016/j.ultrasmedbio.2017.08.004.